Talanta 120 (2014) 398–407

Contents lists available at ScienceDirect

Talanta

journal homepage: www.elsevier.com/locate/talanta

A dual-ion imprinted polymer embedded in sol–gel matrix for the ultra trace simultaneous analysis of cadmium and copper

Bhim Bali Prasad *, Darshika Jauhari, Archana Verma

Analytical Division, Department of Chemistry, Faculty of Science, Banaras Hindu University, Varanasi 221005, India

ARTICLE INFO

Article history:
Received 8 November 2013
Received in revised form
13 December 2013
Accepted 16 December 2013
Available online 22 December 2013

Keywords:
Dual-template ion imprinted polymer
Sol–gel
Nano-film
Metal ions
Differential pulse anodic stripping voltammetry
Simultaneous ultra trace analysis

ABSTRACT

In simultaneous determination of group of elements, there are inter-metallic interactions which result in a non-linear relationship between the peak current and ionic concentration for each of the element, at bare (unmodified) electrode. To resolve this problem, we have resorted, for the first time, to develop a modified pencil graphite electrode using a typical ion imprinted polymer network (dual-ion imprinted polymer embedded in sol–gel matrix (inorganic–organic hybrid nano-material)) for the simultaneous analysis of a binary mixture of Cd(II) and Cu(II) ions, without any complication of inter-metallic interactions and competitive bindings, in real samples. The adequate resolution of differential pulse anodic stripping voltammetry peaks by 725 mV (cf, 615 mV with unmodified electrode), without any cross-reactivity and the stringent detection limits as low as, 0.050 and 0.034 ng mL^{-1} ($S/N=3$) for Cd(II) and Cu(II) ions, respectively by the proposed sensor can be considered useful for the primitive diagnosis of several chronic diseases in clinical settings.

1. Introduction

Cadmium is a toxic heavy metal of continuing occupational and environmental concern with a wide variety of adverse effects [1]. Normal blood Cd(II) is <5.0 ng mL^{-1}, with most results in the range of 0.5–2.0 ng mL^{-1}. Acute toxicity is observed when the Cd(II) level in blood exceeds 50 ng mL^{-1} manifesting *Itai Itai*, high blood pressure, anemia, pulmonary fibrosis, prostrates cancer, lung cancer, yellow discoloration of front teeth near gum line and anosmia [2–4]. Copper, on the other hand, is an essential trace element in biological systems and living organisms [5,6]. Normal Cu(II) level in endogenous (original) blood serum is in the range of 700–1500 ng mL^{-1} [7]. Copper deficiency though very rare, yet it is known to cause various hematological and neurological disorders along with malnutrition, hypoproteinemia, malabsorption, nephrotic syndrome, Menkes disease (a fatal genetic disorder), and microcytic type anemia [8–11]. It is one of the most widespread heavy metal contaminants in environment. The excess of Cu(II) may entail symptoms of gastroenteritis, tissue injury and oxidative damages to biological systems [12]. The World Health Organization (WHO) reported tolerable weekly intakes of Cd(II) and daily intake for Cu(II) as 0.007–0.5 mg kg^{-1} body weight, respectively, for all human groups [13,14]. Obviously, this warrants to measure Cd(II) and Cu(II) ions simultaneously and rapidly in the same sample with a single measurement in various fields like clinical chemistry and/or industrial control. The situation is more aggravated due to low concentration of these metals in the presence of concomitant diverse ions in food and biological samples; and moreover, copper reportedly affect the cadmium peak current and their peak potentials due to inter-metallic formation at the electrode surface [15,16]. Thus, the development of a new method for quantifying trace metals selectively and simultaneously without facing problems of inter-metallic interactions, cross selectivity and interferences, is required and that is a challenging task.

Most of the sophisticated methods recently available for the simultaneous determination of Cd(II) and Cu(II) ions, such as inductively coupled plasma-atomic emission spectroscopy (ICP-AES), ICP-mass spectroscopy, graphite furnace atomic spectroscopy, and neutron activation analysis, are too expensive to be used in routine analysis [13]. Electrochemical methods, on the other hand, have several advantages in terms of their simplicity, fast response, and suitability for the preparation of inexpensive and portable devices. Various electrodes used for this purpose in recent years include hanging mercury drop electrode (HMDE) [15,17–25], Hg coated other electrodes [26–28], modified carbon paste electrodes [29–31], and graphite electrode [32]. Whereas mercury electrodes are not eco-friendly, the solid electrodes might suffer from cross-interferences and inter-metallic interactions in the detection of heavy metals [29–32].

With the inception of the concept of traditional molecular imprinting with a single template, one can think of preparing

* Corresponding author. Tel.: +91 9451954449; fax: +91 5422268127.
E-mail address: prof.bbpd@yahoo.com (B. Bali Prasad).

0039-9140/$ - see front matter © 2013 Elsevier B.V. All rights reserved.
http://dx.doi.org/10.1016/j.talanta.2013.12.036

double-template imprinted materials that have the ability for the simultaneous adsorption of both targets into their respective specific cavities, without any non-specific adsorptions [33–42]. Simply put, molecularly imprinted polymers (MIPs) are highly stable cost-effective materials involving interactions between template molecules and functional monomers through hydrogen bonds or Van der Waals interactions. In the similar norms, ion imprinted polymers (IIPs) have been introduced which required a suitable ligand to form a complex with the metal ion to produce selective binding sites after metal leaching [43,44]. To expand the practicability of IIPs toward simultaneous trace analysis, a preliminary study with aqueous sample, using more than one metal ions as templates in a single IIP format, has already been initiated from our laboratory [45]. However, the coating of such format directly on to the pencil graphite electrode (PGE) surface drastically suffered from the shrinkage and de-lamination of the film after drying. Also, the ensuing complications of inter-metallic interactions and real matrices have never been attended [45]. However, in the present work, the simultaneous determination of a binary group of elements, Cd(II)–Cu(II), using differential pulse anodic stripping voltammetry (DPASV) has been made, for the first time, to alleviate the attendant problems of film de-lamination and inter-metallic interactions, encountered during the course of analysis, in aqueous and real samples. Although the simultaneous analysis of a group of analytes in a single sample has wide practicability to real sample analysis in terms of time and cost-savings, this challenging task can be accomplished through dual-ion imprinted polymer-based sensing materials. Such materials might favor highly selective and sensitive adsorptions of metal ions in their respective ionic cavities amidst massive interferences from diverse ions and false-positives from the complicated matrices of real samples.

In this work, a typical biocompatible monomer (2-acryl amidoethyldihydrogen phosphate), a trapped ligand (L-histidine (L-his)), cross-linker and initiator were thermo-polymerized, in the presence of metal ions. The imprinted polymer was subsequently embedded in a sol–gel matrix (binder) and coated over the surface of PGE. Herein, the inorganic–organic hybrid nano-film with interspersed carbon black powder was found quite competent to behave as 'molecular wire', connecting top IIP-layer and electrode surface to facilitate conductivity and effective transduction of binding event [46].

2. Experimental

2.1. Materials and reagents

Demineralized triple distilled water (conducting range 0.06–0.07 $\times 10^{-6}$ S cm^{-1}) was used throughout the experiment. L-his, acryclic acid, 2,2-azoisobutyronitrile (AIBN), and carbon black powder (1–2 μm), were purchased from Loba chemie (Mumbai, India). Solvents, dimethyl sulphoxide (DMSO) and ethanol were purchased from Spectrochem Pvt. Ltd. (Mumbai, India). Ethylene glycol dimethacrylate (EGDMA), tetraethyl orthosilicate (TEOS), and 2-aminoethyldihydrogen phosphate were provided by Fluka (Steinheim, Germany). Copper sulfate, cadmium sulfate, ethylenediamine tetraacetic acid disodium salt (EDTA), and all interferents were purchased from E-Merck Ltd. (Mumbai, India). All chemicals were of analytical grade and used without further purification. Acetate buffer solution (pH 5.0, ionic strength 0.1 M), was used as a supporting electrolyte. The pH values of test solutions were adjusted by addition of a few drops of either 0.1 M HCl or 0.1 M NaOH. Standard stock solutions of copper sulfate and cadmium sulfate (500.0 μg mL^{-1}) were prepared in water. All working solutions were prepared daily by diluting stock solution with water.

Pharmaceutical sample, Amino-fit (soflet®) tablet, was purchased from Universal Pvt. Ltd. (Mumbai, India). Lake water samples were obtained from the vicinity of local area. Cow's milk was collected from a local dairy in nitric acid-washed glass vials and a drop of concentrated hydrochloric acid was added to preserve its oxidation status. Human blood serum was obtained from the Institute of Medical Science, Banaras Hindu University (Varanasi, India). Both milk and serum samples were brought in ice packs for further processing in the laboratory, where they were kept at ~4 °C, till use. Any pre-treatment of real sample (ultra filtration, ultra centrifugation, de-proteinizations etc.) was deliberately avoided since it may lead to inaccuracies in ultra trace analysis. Instead, requisite dilutions of these samples were required to move the analysis in the practical range of the proposed sensor and also, by and large, to mitigate the matrix effect.

Pencil rods (2B), 0.5 mm in diameter and 5 cm in length, were purchased from Hi Par, Camlin Ltd. (Mumbai, India). The PGE was used because of its large electrode active surface area, high electrochemical activity, good mechanical stability, low cost, low background current, and wide potential window.

2.2. Apparatus

All voltammetric measurements were carried out on a polarographic analyzer/stripping voltammeter [model 264 A, EG & G Princeton Applied Research (PAR), USA] in conjunction with an electrode assembly (PAR model 303A) and an X–Y chart recorder (PAR model, RE 0089). Chronocoloumetry measurements were carried out with an electrochemical analyzer (CH instruments, USA, model 1200 A). All experiments were performed using a three electrode cell assembly consisting of dual-ion imprinted polymer embedded in sol–gel matrix/PGE (sol–gel–DIIP/PGE), platinum wire, and Ag/AgCl (3.0 M KCl) as working, counter, and reference electrodes, respectively. IR spectral studies were made using Varian 3100 FTIR (USA). Thermo-gravimetric analysis (TGA) of sol–gel–DIIP-template adduct and DIIP was carried out with a Perkin Elmer-STA 6000 (USA) Surface morphologies of the coatings were studied with scanning electron microscope (SEM), JEOL, JSM model-840 A (Netherland), and atomic force microscope (AFM) (using a NT-MDT microscope, NT-MDT Co., Russia) in the semi contact mode. All experiments were carried out at 25 ± 1 °C.

2.3. Synthesis of monomer (2-acrylamido ethyl dihydrogen phosphate, AEDP)

The monomer used in this work was a typical biocompatible acryl phosphate, structurally akin to phosphoethanolamine-a precursor of phospholipid synthesis, that could effectively bind Cd(II) and Cu(II) ions both in vivo/vitro conditions. For this, the monomer, AEDP, was most suitably synthesized following a known recipe [47]. In brief, 400 μL acrylic acid was added drop wise to an alkaline solution of 2-aminoethyldihydrogen phosphate (0.71 g/4.0 mL 1.0 N NaOH) with continuous stirring for ~3 h. After evaporating water, a white crude product was obtained which was re-crystallized by ethanol and characterized by FT-IR. [FT-IR (KBr), ν_{max} (cm^{-1}): 3465 (–NH stretch), 1659 (–C=C vinyl stretch), 1641 (amide C=O stretch), 1562 (amide N–H bending), 1424 (P=O), 1318 (P–O–C), and 985 (P–OH)].

2.4. Synthesis of dual-ion imprinted polymer (DIIP)

For the preparation of DIIP-adduct, a mixed DMSO solution of template ions and monomer (0.05 mmol of each template (Cd(II), 0.038 g/250 μL and Cu(II), 0.012 g/250 μL) and 0.15 mmol AEDP monomer (0.027 g/500 μL DMSO) (Cd: Cu: AEDP=1: 1: 3)) and 0.1 mmol ligand, L-his (0.016 g/250 μL DMSO), were taken together in a glass vial followed by intermittent shaking for

30 min at room temperature to allow the formation of a stable complex between monomer, metal ions, and ligand. Afterward, 0.037 mmol of AIBN (0.006 g/0.100 μL DMSO) and 2.25 mmol cross-linker (EGDMA, 423 μL) were mixed to this complex to get a homogeneous admixture. The whole content was deoxygenated with N_2 gas for 10 min. The glass vial was sealed and cured in an oven at 60 °C for 3 h for thermal polymerization. The polymer so obtained was ground and sieved to particle size 10–15 μm. Complete removal of template was made to obtain DIIP by washing the polymer-adduct by EDTA (0.1 M), under dynamic condition for 30 min, until no voltammetric signal was noticed for both the ions. Non-imprinted polymer (NIP) was also obtained under the same conditions, but in the absence of the templates (Cd (II) and Cu(II)).

2.5. Electrode preparation and voltammetric procedure

The pencil graphite rod was first pretreated with 6 M HNO_3 for 15 min, followed by water-washing. After smoothening its surface by soft cotton, this was inserted into a Teflon tube. Any micro-gaps in between the graphite rod and the tubing were sealed properly with the help of an epoxy spray. The tip of the pencil rod at one end was gently rubbed with an emery paper (No. 400) to level the pencil surface along the tube orifice. Electrical contact was made by soldering a metallic wire to the exposed reverse side of the pencil rod.

The sol–gel used in the sensor preparation serves as binders to hold DIIP layers at exterior surface. For this a clear sol–gel solution was obtained by stirring a mixture of 1.0 mL TEOS, 1.0 mL ethanol, 0.5 mL water, and 0.05 mL HCl (0.1 M) for 30 min. This was left to gel for another 45 min so as to reach to 'synersis' stage (a stage between ageing and drying of gel). To prepare the sol–gel–DIIP/PGE, 1.0 mL sol–gel solution, 300 μL of 1500 μg mL^{-1} DIIP (0.015 g/1.0 mL DMSO), and an optimized amount of carbon black powder (10 mg) were mixed together by mechanical stirring for 10 min, and 15.0 μL of this mixture was spin coated over PGE surface at 2600 rpm for 60 s. The use of carbon black powder in the coated film helped restricting its shrinkage and enhancing conductivity, on account of its homogenous dispersion in the viscous silicate network. The modified electrode was kept overnight for drying in a desiccator. The sol–gel–NIP/PGEs were also prepared following the same procedure.

Both bare and sol–gel–DIIP/PGEs were immersed in to the cell containing 10.0 mL acetate buffer (pH 5.5). After recording blank run, aliquots of freshly prepared solutions of Cd(II) and Cu(II) were added (a) one by one, (b) one in excess of another, and (c) simultaneously, in the cell for analyte accumulation at −1.2 V (respective to Ag/AgCl) for 150 s. After analyte(s) accumulation, DPASV runs were recorded in the potential range varying from −1.2 to +0.4 V, at scan rate 10 mV s^{-1}, pulse amplitude 25 mV, and pulse width 50 ms. Cyclic voltammetry (CV) experiments were also performed within the same potential window at various scan rates (ν) (10–200 mV s^{-1}) in anodic stripping mode. Since oxygen did not influence the analyte(s) oxidation, deaeration of the cell content in this work was not required. The limit of detection (LOD) was calculated as three times the standard deviation for the blank measurement (in the absence of Cd(II) and Cu(II)) divided by the slope of the calibration plot [48]. DPASV runs were also recorded on sol–gel–NIP-PGE under identical operating conditions.

3. Results and discussion

3.1. Role of ligand (L-his)

Biocompatibility of histidine toward the complexation of transition metal ions in biological systems has already been proven using different techniques [49–56]. The involvement of Cu (II)–L-his complex in copper transport in blood plasma reflects its high stability [54,55]. Cadmium on the other hand, is known to form complexes with all natural amino acids and peptides. The coordination geometry of metal complexes is generally octahedral with the involvement of the amino and carboxylate groups of the ligand in metal binding [56]. Accordingly, it is shown that L-his binds to Cd(II) and Cu(II) through the amino and imidazole groups in the chelate plane and through the carbonyl group in the apical position. Based on this, the development of L-his-template(s)-monomer interactions and spatial arrangement of DIIP-cavities for Cd(II) and Cu(II) are suggested in Scheme 1(A).

The binding interactions between the metal ions with L-his were examined in order to prove the proposed geometry. The stability

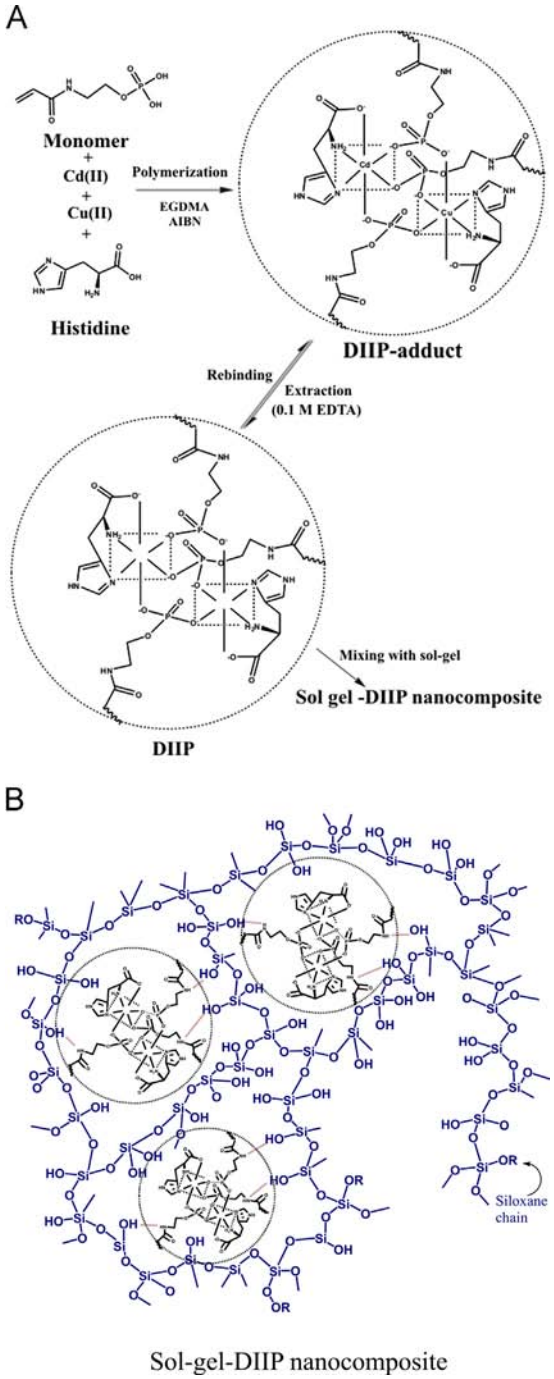

Scheme 1. Suggested mechanisms for: (A) Cd(II) and Cu(II) bindings simultaneously in their respective imprinted cavities and (B) sol–gel–DIIP nano-material.

constants (β) of L-his with Cd(II) and Cu(II), were calculated on the basis of an empirical equation [57]:

$$\frac{1}{ip} = \frac{1}{ip,\ max} + \frac{1}{ip,\ max\,\beta\ C_t^{\,m}} \quad (1)$$

where i_p is the measured peak current, $i_{p\ max}$ the peak current when all template molecules formed complex with IIP cavity, C_t is the concentration of template, m is the coordination number of the complex formed between template and metal ion. By plotting $1/i_p$ versus $1/C_t^m$ for different 'm' values, a straight line was constructed for the corresponding complex. Our calculations showed that when $m=1$ for Cd–L-his and Cu–L-his complexes, perfect straight lines with $R^2=0.99$ in each case were obtained. This suggested that each metal ion was bound to one L-his ligand. In other words, the ligand L-his might serve as a promoter, through stable metal complexation, to form a rigid structure consisted of L-his-metal ion-monomer, obviating any disturbances caused by the water in rebinding experiments. The stability constants (β) of Cd–L-his and Cu–L-his complexes were found to be 1.7×10^{-3} and 2.8×10^{-3}.

Insofar as suitability of L-his as a ligand in the present instance is concerned, we have examined various amino acids (which are known to strongly complex with both the template ions) through UV–vis spectroscopy. For this, each amino acid is mixed with Cd(II) and Cu(II) in 2:1:1 ratio in DMSO and their absorption spectra were recorded (Fig. S1(A)). Accordingly, the absorption maxima were found around 650–800 nm for various complexes in the order: histidine > cysteine > glycine. Therefore, L-his was found to be most appropriate one for use in this work.

3.2. Spectroscopic evidence on stoichiometry of L-his-template(s)

The complexation of L-his with Cd(II) and Cu(II) at different metal/ligand ratios was investigated by UV–vis spectroscopy. Accordingly, as the molar concentrations of $CdSO_4$ and $CuSO_4$ were kept constant and L-his increased, the intensity of maximum absorbance at 600 nm increased gradually till it attained an optimum absorption intensity, at molar ratio between $CdSO_4$ (0.5 mmol), $CuSO_4$ (0.5 mmol), and L-his (1.0 mmol) equal to 1:1:2, and thereafter started decreasing with further increase in molar concentration of L-his (Fig. S1(B)). Also, a red shift was observed for higher ligand concentrations, probably due to binding of more than 1 mol of L-his to the single mol of metal ion(s) leading to higher extent of electron delocalization from the d orbitals of metal to the ligand [58]. On the other hand, keeping ligand concentration constant and increasing concentration of both metals always revealed absorption peak with decreased intensity, probably due to incomplete complexation. Moreover, when the molar concentrations of $CdSO_4$ and $CuSO_4$ were mutually varied while L-his kept constant, the optimum intensity of maximum was only noticed when molar ratio of $CdSO_4$ (0.5 mmol), $CuSO_4$ (0.5 mmol) and L-his (1.0 mmol) was specifically 1:1:2 (Fig. S1(C)). This indicates that each metal complexes with one ligand. At other metal concentrations, low absorbance was observed with broad peaks. Accordingly, as many as three coordination sites of both the metal ions are occupied by one molecule of L-his (via complexing with carboxylate group, amino group, and imidazole nitrogen atom), and remaining three have to be occupied by phosphate groups of three discrete molecules of monomer (Scheme 1 (A)).

3.3. Characterization of coated film

FT-IR spectra (KBr) (Fig. S2) of sol–gel (curve A), monomer (curve B), DIIP-adduct immobilized sol–gel (curve C), sol–gel–DIIP (curve D), and NIP-sol–gel (curve E), were comparatively studied to explore binding mechanism. FT-IR peaks of pure sol–gel (–OH stretch due to silanol group (3443 cm^{-1}), Si–O–Si bridge (1080 cm^{-1}), Si–OH stretch (948 cm^{-1}), curve A) remained intact in all the spectra (curves C–E) The bands, due to monomer (P–OH (985 cm^{-1}), curve B) and L-his (–NH (3125 cm^{-1}), C=O (1730 cm^{-1}), and –C=N– of imidazole ring (1570 cm^{-1})) were shifted downward [930, 3050, 1700, and

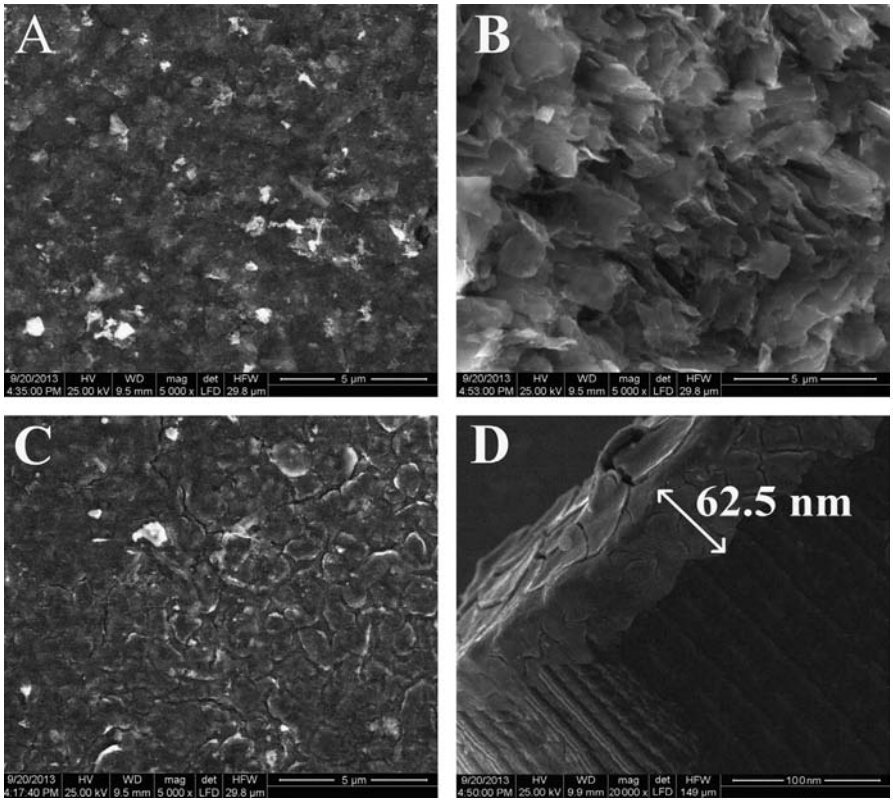

Fig. 1. SEM images: (A) sol–gel–DIIP-adduct/PGE, (B) sol–gel–DIIP/PGE, (C) sol–gel–NIP/PGE, and (D) side view of sol–gel–DIIP/PGE.

1480 cm^{-1}], on complexing with templates (Cd(II) and Cu(II)) in final adduct (Fig. S2, curve C). This may be attributed to the co-ordination between the metal ions, monomer and trapped ligand. Also, the band corresponding to vinyl group in monomer (1659 cm^{-1}) disappeared in the polymer (curves C, D and E) indicating complete polymerization of the monomer. Notably, amide bands (amide I (amide C═O stretch), amide II (amide N–H bending)) of the monomer used remained unaffected after polymerization (curves B–E). Furthermore, the above observed changes in –NH, C═O, C═N and P–OH stretching frequencies after template binding reinstated to their respective original positions in the sol–gel–DIIP (curve D). This suggests complete retrieval of templates. Based on these observations, one may infer that (1) both ligand and monomer were bonded to the metal ions and (2) the ligand remained in the polymer matrix while the template(s) were extracted. Interestingly, the P═O band (1430 cm^{-1}) of monomer remained unaltered in both DIIP-adduct and DIIP, and as such did not participate in metal binding. Sol–gel–NIP expectedly showed a similar spectrum as observed with sol–gel–DIIP. Interestingly the Si–OH broad peak of sol–gel (curve A) and –NH stretching vibration of the monomer (curve B), both appearing around 3465 cm^{-1} (broad) were turned to be relatively sharp at slightly downward position in the sol–gel–DIIP and sol–gel–NIP, in curves C, D, and E, respectively. This may be attributed to the hydrogen bonding (Scheme 1(B)) between amide groups of AEDP and hydroxyls of inorganic oxide of the sol–gel used as binder [59].

The DIIP-adduct was found thermally stable upto 470 °C, whereas DIIP was stable upto 590 °C. This may be attributed to the complexation effect in DIIP-adduct (For details, vide Supplementary material section S1 and Fig. S3).

SEM images (Fig. 1) at 5000 × magnification depict the surface morphology of modified electrodes. Accordingly, the sol–gel–DIIP-template-adduct coating on PGE surface was apparently porous but largely compact owing to the carbon dispersion with no cracks (Fig. 1A). Interestingly, this film turned to be highly porous with vertical tethering on the lateral surface, after metal ions retrieval (Fig. 1B). The appearance of such tethered flakes (brush) of nano-material might offer a channelized electron transport from top to bottom amidst carbon powder, representing pores with increased contact area and apertures of different depths that favored film wettability and electrical conductivity throughout the film texture. The corresponding NIP surface, on the other hand, lacked any vertical tethering showing literally a compact texture without any pores (Fig. 1C). Fig. 4D displays the side view of the SEM image (20,000 × magnification) of a cross-section of sol–gel–DIIP/PGE reflecting the thickness of coating to be 62.5 nm.

Surface morphologies were further examined using AFM (three-dimensional) images recorded under semi contact mode for sol–gel–DIIP/PGE (Fig. 2A) and sol–gel–DIIP-adduct/PGE surfaces (each showing 25 μm^2 area studied) (Fig. 2B). Although the DIIP-adduct coating was largely uniform, the elevated bumps of sol–gel seen hither and thither generated porosity to some extent. The arithmetic mean roughness (Ra), root mean square roughness (Rq), and surface height (Rz) of this texture were observed to be 2.3, 3.2 and 91.2 nm, respectively (Fig. 2B). On the other hand, after metal ions (templates) removal, the coated layer assumed Ra and Rq values of 3.9 and 5.0 nm, respectively and surface height about 82.0 nm (Fig. 2A). The increase of surface-height on adduct formation vis-à-vis DIIP reflects the template embedded structure. An average thickness of sol–gel–DIIP film on PGE surface was calculated to be 62.2 nm using the following equation [60]:

$$z(x,y) = s(x,y) + t + \Delta z(x,y) \quad (2)$$

where $z(x,y)$ is the surface-height (82.0 nm) of sol–gel–DIIP/PGE, $s(x,y)$ is the surface-height (14.8 nm) of bare PGE [61], t is the average thickness, and $\Delta z(x,y)$ is the inherent roughness

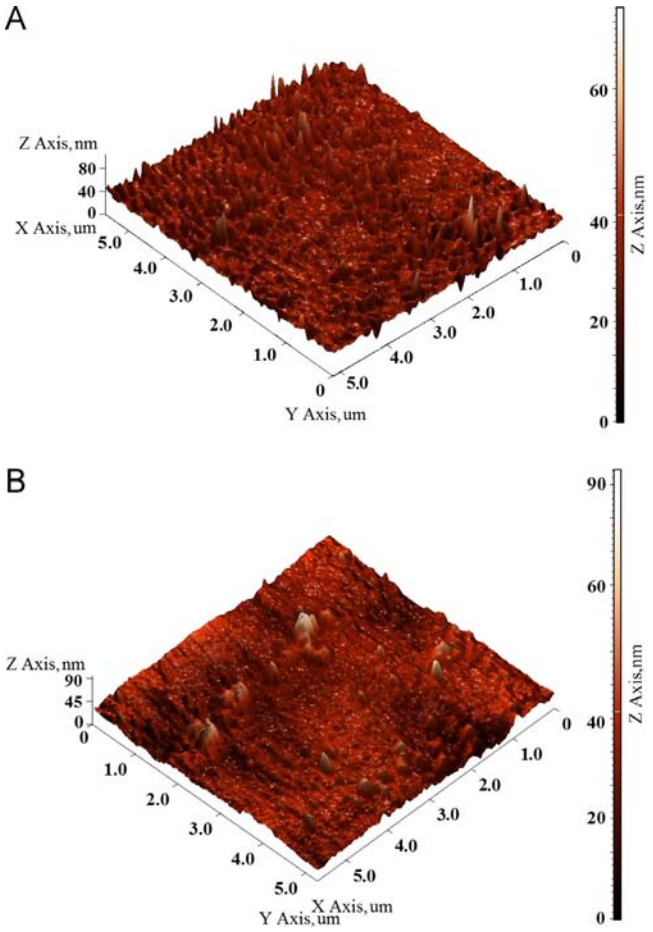

Fig. 2. AFM images: (A) sol–gel–DIIP/PGE and (B) sol–gel–DIIP-adduct/PGE.

(Rq = 5.0 nm) of DIIP film. The calculated value of mean thickness (t) of coating was found to be very close to that obtained by SEM.

3.4. Factors affecting sensor development

In order to ensure the best results, modified PGE was examined for its imprinting performance. Of the various factors that have been identified for the formation and the recognition properties of binding sites, multiple site interactions with the functional monomers are likely to yield binding sites of high specificity and affinity. The binding strength of polymer (as well as the fidelity in the recognition) depends on number and type of interaction sites, the template shape and the monomer-template rigidity. Thus, a better fit between the site and the template leads to less entropy loss due to the conformational changes in the site as well as in the template upon rebinding. In this work, a number of electrodes using different molar ratios (1:1:1, 1:1:2, 1:1:3 and 1:1:4) of both the templates and monomer were developed. Of all, the molar ratio of 1:1:3 responded a maximum development of the DPASV current response; other revealed lower response either owing to decline in the number of binding sites in the absence of adequate amount of monomer (hence improper complexation with the template ions in the polymer chain); or the probable heterogeneity of binding sites in the presence of an excess amount of monomer. Furthermore, the DPASV peak current increased with cross-linker amount up to 2.25 mmol and then decreased gradually. The decreasing current is presumably due to a very rigid polymer network above 2.25 mmol which restricts an easy access of the template molecule to binding sites. (For details on the optimization of conditions for electrode modification, vide Supplementary material Section S2).

For the comparative study, different kinds of modified PGEs (including bare PGE) using various coatings, viz., sol–gel, dual-ion imprinted sol–gel (sol–gel matrix imprinted for Cd(II) and Cu(II) ions), sol–gel–NIP and sol–gel–DIIP, all with embedded carbon powder, were prepared. Direct DIIP coating on bare electrode was not stable since the coated layer was found to be crippled down, after drying. As shown in Fig. S4 (A), DPASV responses with only sol–gel and NIP-modified electrodes were found to be non-responsive for both the analytes (curves b and c), while dual-ion imprinted sol–gel/PGE showed somewhat restricted response (curve d). A drawn-out (curve e) response was noticed with unmodified PGE. However, the activity of sol–gel–DIIP/PGE was significantly enhanced showing specific binding of both analytes, with linear response in both ranges of lower and higher concentrations (curves f, h). DPASV curves *a*, *g*, and *i* represent blank, spiked Cd(II), and spiked Cu(II) runs recorded on sol–gel–DIIP/PGE, respectively.

3.5. Binding isotherm

The binding interaction between the polymer and the templates can be described as Cd(II)+Cu(II)+DIIP $\overset{K_a}{\rightleftharpoons}$ Cd–DIIP–Cu. This equilibrium can better be represented by a Langmuir adsorption isotherm on the basis of following equation [62]:

$$\frac{C_0}{I}=\frac{1}{I_{max}K_a}+\frac{C_0}{I_{max}} \quad (3)$$

where I is the DPASV current-height based on the amount of analyte(s) bound to the polymer and C_0 is the concentration of free analyte(s) molecules in the solution, approximated to the analytical concentration. I_{max} articulates maximum current connoting the maximum number of binding sites, K_a $(=1/K_D)$ represents equilibrium binding constant, and K_D is the equilibrium dissociation constant of DIIP-adduct. Accordingly, a linear equation, $C_0/I=(0.077\pm0.005)\ C_0+(0.039\pm0.015)$ ($R^2=0.99$), for the plot of C_0/I vs. C_0 is obtained for Cd(II). Simultaneously, Cu(II) responded a linear equation, $C_0/I=(0.042\pm0.001)\ C_0+(0.026\pm0.001)$ ($R^2=0.99$). The K_D and I_{max} values thus estimated are: 0.515 and 12.91 μA for Cd(II) and 0.513 and 20.12 μA for Cu(II), respectively. The Gibbs free energy change ($\Delta G=-\mathrm{RT}\ln K_a$) due to adsorption is calculated as -1.65 kJ mol^{-1} for both analytes; the negative values of ΔG indicates spontaneous adsorption of the analytes. The perfect linearity of the isotherms implies the existence of a homogenous population of sites for the imprint molecules in the coated film. Thus, the coated layer could serve as an ideal adsorbent with identical and small K_D values for both metal ions, and thereby demonstrating a better association (binding affinity).

3.6. Inter-metallic effect

There were contradictory reports about the existence of a Cu-Cd inter-metallic compound. Some studies have noted a depression of cadmium stripping wave [15,16,63,64] due to Cu-Cd inter-metallic formation at the electrode surface and some summarily rejected this concept [65,66]. However, in the present instance, the Cu–Cd inter-metallic compound formation was prominent at bare solid electrode (PGE) that observed mutual interferences on peak currents of both metal analytes at higher concentrations. Copper in simultaneous mixture had shown more pronounced effect on cadmium DPASV peak as compared to the effect of cadmium on copper (Fig. S5). Fortuitously, it was observed that Cu–Cd inter-metallic formation is minimal or non-existent when modified PGE was used; thanks to the phenomenal imprinting effect generating specific cavities of Cu(II) and Cd(II) which have high propensity toward independent binding kinetics, without any cross-interference. Despite the fact that both metal ions have identical binding affinity to capture their respective cavities, Cu(II) ions always revealed higher measurement sensitivity (slopes of linear concentration range: 16.980 and 3.514 with modified PGE and bare PGE, respectively, Table 1). This was primarily because of 4-fold higher diffusion coefficient for Cu(II) as compared to Cd(II) for oxidative stripping on sol–gel–DIIP/PGE (Table S1) This could the reason that slopes of cadmium measurements were inferior to copper in DPASV measurements (Table 1). However, the correlation coefficient with modified PGE was 0.99 (perfect linear) whereas the same for bare electrode was less than 1 for both metal ions (Table 1). This reflects severe involvement of inter-metallic interferences at bare PGE. On the other hand, Cu–Cd inter-metallic bond was drastically weakened favoring Cu–Cd inter-metallic compound to be readily dissolved, under the influence of strong and independent binding interactions exhibited by the respective cavities of both metal ions. In this way, the long standing crucial problem of inter-metallic between Cd(II) and Cu(II) was fully resolved by the proposed sol–gel–DIIP/PGE.

3.7. Electrochemical studies

For electrochemical studies, all operating conditions such as accumulation potential (E_{acc}), accumulation time (t_{acc}), and pH of the test solution were optimized on sol–gel–DIIP/PGE (For details, vide Supplementary material section S3). Electrodics of the proposed sensor for Cd(II) and Cu(II) was studied with the help of CV, recorded in anodic stripping mode, at different scan rates in acetate

Table 1
Analytical results of DPASV measurements on sol–gel–DIIP–sol gel/PGE in aqueous samples.

Analyte/s	Regression equation	Linear range (ng mL^{-1})	LOD[a] (ng mL^{-1})	RSD[b](%) ($n=3$)
Cd(II)	$I_p=(3.917\pm0.016)\ C+(0.145\pm0.056)$, $n=13$, $R^2=0.99$	0.125–5.942	0.051	0.39
Cu(II)	$I_p=(16.819\pm0.017)\ C+(0.019\pm0.017)$, $n=7$, $R^2=0.99$	0.125–1.799	0.036	0.16
Cd(II) and Cu(II) mixture				
Cd(II)	$I_p=(3.729\pm0.087)\ C+(0.029\pm0.179)$, $n=8$, $R^2=0.99$	0.124–2.989	0.053	2.43
Cu(II)	$I_p=(16.980\pm0.753)\ C+0.249\pm0.359)$, $n=8$, $R^2=0.99$	0.124–0.725	0.035	4.39
Cd(II) (with 1.715 ng mL^{-1} Cu(II), fixed)	$I_p=(4.055\pm0.001)\ C+(0.010\pm0.015)$, $n=7$, $R^2=0.99$	0.429–4.305	0.049	0.02
Cu(II) (with 2.621 ng mL^{-1} Cd(II), fixed)	$I_p=(16.942\pm0.002)\ C\ +(0.028\pm0.063)$, $n=6$, $R^2=0.99$	0.146–1.369	0.0354	0.02
Cd(II) and Cu(II) Mixture[c]				
Cd(II)	$I_p=(0.489\pm0.162\ )\ C+(0.610\pm0.368)$, $n=8$, $R^2=0.75$	0.495–1.449	0.053	2.43
Cu(II)	$I_p=(3.516\pm0.393)\ C+(0.721\pm0.358)$, $n=8$, $R^2=0.96$	0.124–0.542	0.035	4.39

[a] LOD based on the minimal distinguishable signal for lower concentration of analyte.
[b] RSD (%) for three sets of LOD data.
[c] DPASV measurements on bare PGE in aqueous samples.

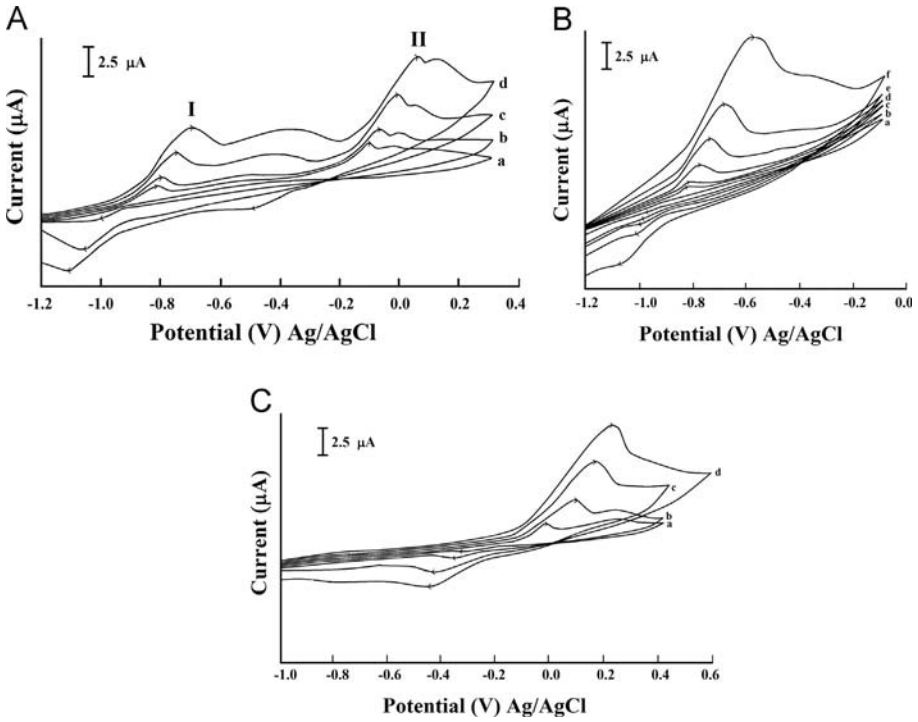

Fig. 3. CV for (A) simultaneous determination of Cd(II) (1.50 ng mL^{-1}) and Cu(II) (0.51 ng mL^{-1}) at different scan rates: (a) 10, (b) 20, (c) 50, (d) 100 mV s^{-1}, (B) individul Cd(II) (1.80 ng mL^{-1}) at different scan rated (a–f, 10-500 mV s^{-1}), and (C) individual Cu(II) (0.84 ng mL^{-1}) at different scan rates: (a) 10, (b) 20, (c) 50, and (d) 100 mV s^{-1}, recorded in anodic stripping mode, on sol–gel–DIIP/PGE.

buffer (pH 5.5). Both metal ions were accumulated simultaneously with identical binding affinities, at E_{acc} −1.20 V (vs. Ag/AgCl) for 150 s (t_{acc}), in their respective cavities, under the influence of electrostatic interactions, and thereafter instantly reduced to uncharged metals (Cd^0, Cu^0). Subsequently, the entrapped analytes were allowed to strip off anodically after 15 s equilibration. This resulted in two pairs of a redox current (peak I for Cd(II) and peak II for Cu(II)), with potential separation ($\Delta E_p = E_{pc} - E_{pa}$) of 400 mV for Cd(II) (1.50 ng mL^{-1}) and 464 mV for Cu(II) (0.51 ng mL^{-1}) on DIIP-sensor at scan rate 100 mV s^{-1} (Fig. 3A). Interestingly, the CV runs when recorded exclusively with Cu(II) (Fig. 3C), displayed cathodic peak in reverse scan even at a low scan rate ($\nu = 10$ mV/s), whereas in a mixture of both analytes, its cathodic peak appeared only at higher scan rate ($\nu = 100$ mV/s) (Fig. 3A). This may be attributed to the availability of Cd(II) and Cu(II) as stripped oxidized ions at the electrode surface to recombine as Cu(II)-Cd(II) inter-metallic compound that was not accessible for reduction in sufficient time scale in the reverse scan at lower scan rates. Instead, the oxidized product (Cu(II)–Cd(II) inter-metallic) has been adsorbed at the electrode surface, as revealed by the emergence of a broader pre-peak. The minor post-peak to copper emerges due to partial oxidation of stripped Cu^0 to Cu(I) which remained complexed to cavity rather than being dissolved in the solution [67]. The above effect was not perceivable whether CV recorded for cadmium individually (Fig. 3B) or with copper (Fig. 3A); in this case well resolved anodic-cathodic peaks were observed at all scan rates.

Interestingly, both analytes observed quasi-reversibility at sol–gel–DIIP/PGE. The oxidation peaks, in stripping mode, for both metals shifted positively with scan rates. This was due to the apparent difficulty in striping process in short duration, and thus required a higher energy for the oxidation with the increase of scan rates. Notwithstanding the fact that inter-metallic formation might re-emerge in the reverse scan of CV, the electro-oxidations were purely of diffusion controlled nature. This could be evinced from following linear relationships between peak current (I_{pa}) vs square root of scan rate ($\nu^{1/2}$) as:

$$\text{Cd} : I_{pa} = (-1.156 \pm 0.300) + (13.089 \pm 0.784)\nu^{1/2} \quad (R^2 = 0.99) \tag{4}$$

$$\text{Cu} : I_{pa} = (-3.949 \pm 0.319) + (11.829 \pm 1.503)\nu^{1/2} (R^2 = 0.99) \tag{5}$$

One may also estimate the electron-transfer rate constant (k) on the modified electrode ($n\Delta E_p < 200$ mV, $\Delta E_p = Ep_a - E_{pc}$) using Laviron equation [68]:

$$\log k = \alpha \log(1-\alpha) + (1-\alpha)\log\alpha - \log\left(\frac{RT}{nF\nu}\right) - \alpha(1-\alpha)nF\Delta E_p/2.3RT \tag{6}$$

where α is the electron-transfer coefficient, F is the Faraday constant, ν the scan rate (V s^{-1}), R the gas constant, T the temperature, and n is the number of electron transfer. The values of n are obtained as 2.1 and 2.0 for cadmium and copper, respectively through chronocoulometry studies. (For details on chronocoulometry, vide Supplementary material section S4). The α values (0.70 for Cd(II) and 0.87 for Cu(II)) could be obtained from the slope ((2.303RT/(1−α)nF) of E_p vs. log ν plot. Substituting α value in Eq.6 revealed k values for Cd(II) and Cu(II) to be 3.16×10^{-2} s^{-1} and 2.5×10^{-2} s^{-1}, respectively. The fractional α values, which are not far from unity, might suggest prevailing electrodics to be much prone toward reversibility (not perfect reversibility), in the present instance. The sluggish reversibility may be attributed to the blocking effect, partially on the part of surface coverage of the DIIP-film, toward electron-transport.

3.8. Analytical determination

DPASV is better than CV for quantification since this utilizes pulse modulation amplitude of 25 mV and pulse width 50 ms, providing a sufficient time scale for the measurement, without

Table 2
Analytical results for DPASV measurements on sol–gel–DIIP/PGE in real samples.

Sample	Ion/s	Regression equation	Determined value (mean ± S.D) (ng mL^{-1})	LOD[f] (ng mL^{-1})	RSD (%) (n=3)
Tablet (diluted 12.54 × 10^4 fold)	Cu(II)	I_p=(16.754 ± 0.542) C+ (0.395 ± 0.482), n=8, R^2=0.99	0.159 ± 0.001 (199,386 ± 125)[b]	0.035 (4389)	3.2
Human blood serum (diluted 8.02 × 10^3 fold)	Cd(II)[a]	I_p=(3.748 ± 0.039) C+ (0.599 ± 0.334), n=8, R^2=0.99	–	0.053	1.1
	Cu(II)	I_p=(16.982 ± 1.218) C+ (1.234 ± 1.145), n=8, R^2=0.99	0.137 ± 0.001 (1098 ± 1.0)[c]	0.035 (280.7)	4.5
Cow's milk (diluted 1.01 × 10^2 fold)	Cd(II)	I_p=(3.961 ± 0.047) C+0.069 ± 0.107), n=4, R^2=0.99	0.4240 ± 0.002 (42.824 ± 0.2)[d]	0.050 (5.1)	1.2
	Cu(II)	I_p=(16.223 ± 0.194) C+ (0.268 ± 0.199), n=4, R^2=0.99	0.904 ± 0.001 (91.3 ± 0.2)[e]	0.037 (3.7)	1.2
Lake water sample	Cd(II)		Not detected		
	Cu(II)	I_p=(16.332 ± 0.094) C +(0.387 ± 0.078), n=6, R^2=0.99	0.139 ± 0.002	0.034	1.3

[a] The initial concentration of Cd in dilute blood serum could not be determined by the proposed method; however measurements were feasible only after standard additions.
[b] Value in parenthesis denotes endogenous (original) concentration of Cu(II) in tablet obtained by multiplication by dilution factor of 12.54 × 10^4.
[c] Value in parenthesis denotes endogenous (original) concentration of Cu(II) in blood serum obtained by multiplication by dilution factor of 8.02 × 10^3.
[d] Value in parenthesis denotes endogenous (original) concentration of Cd(II) in cow's milk obtained by multiplication by dilution factor of 1.01 × 10^2.
[e] Value in parenthesis denotes endogenous (original) concentration of Cu(II) in cow's milk obtained by multiplication by dilution factor of 1.01 × 10^2.
[f] Data presented in parenthesis refer to the minimum concentration of the initial samples (before dilution) and that could only be measured after requisite dilution and subsequent multiplication by the respective dilution factor.

contributing any charging current to the background current. Therefore, simultaneous estimation of Cd(II) and Cu(II) was carried out, under the optimized conditions of DPASV, using sol–gel – DIIP/PGE sensor in aqueous, pharmaceuticals, human blood serum, cow's milk and lake water samples (Tables 1 and 2). DPASV analysis of Cd(II) and Cu(II) ions in aqueous solutions (0.1 M acetate buffer, pH 5.5, scan rate 10 mV s^{-1}) on sol–gel – DIIP/PGE demonstrated specific and quantitative adsorption of these metal ions in individual capacity (Fig. S4(A)) (For details, vide Supplementary material section S5). However, studies of the influence of Cu(II) on the binding of Cd(II) and vice versa on sol–gel–DIIP/PGE are pertinent under competitive binding conditions in simultaneous analysis. This is due to reported inter-metallic interactions, which results in a non-linear relationship between the peak current and the ionic concentration for each of the elements. Often Cu(II) concentration is found excess than that of Cd(II) in biological fluids. In this context, Cd(II) was kept at a fixed large concentration (2.621 ng mL^{-1}) and the Cu(II) concentration was increased (0.146–1.369 ng mL^{-1}, Fig. 4A, curves a to f) that responded a linear calibration plot (Fig. 4A, inset) between current (I_p, μA) and concentration (ng mL^{-1}). Similarly, Cu(II) was taken at a fixed concentration (1.815 ng mL^{-1}) and Cd(II) concentration increased from 0.429–4.305 ng mL^{-1} [Fig. 4B (curves a–g)] to follow a linear regression (Fig. 4B, inset). Interestingly, excess copper did not affect the cadmium peak current and peak potential. When both Cd (II) and Cu(II) concentrations were simultaneously varied in the mixed solution, symmetrical DPASV peaks were observed at their respective oxidation potentials (without any shifts and mutual competition for binding) with sol–gel–DIIP/PGE (Fig. 4C, curves a–h). The ill-defined post-peaks to DPASV at all concentrations of both metals indicate weak adsorption of reactants (Cd^0 and Cu^0) at electrode surface that are oxidized as tailing peaks around −0.6 V and +0.1 V for $Cd^0 \rightleftharpoons$ Cd(II) and $Cu^0 \rightleftharpoons$ Cu (II) oxidations in stripping mode, respectively. These metal cations after DPASV could not combine as Cu(II)–Cd(II) inter-metallic, unlike what we have proposed in CV. The reason being the stripped cations (Cd(II) and Cu(II)) could readily be dissolved and migrated to bulk solution, rather than being adsorbed on the electrode surface in the form of an inter-metallic combination as proposed particularly before CV reverse scan.

The proposed sensor was validated with real samples. Of these, pharmaceutical tablet and lake water samples contained exclusively Cu(II), whereas cow's milk had both Cd(II) and Cu(II) ions present together. Insofar as human blood serum sample is concerned, it possesses predominantly Cu(II) (500 times larger) concomitantly with traces of Cd(II). Thus, for demonstrating the feasibility of the simultaneous analysis, the original serum sample under investigation has to be fortified with Cd(II) in the quantifiable range detectable by the proposed sensor. Typical DPASV curves for Cu(II) in pharmaceutical and lake water samples, Cd(II) and Cu(II) in blood serum samples and cow's milk, are shown in Fig. S4(B). The corresponding analytical results are shown in Table 2, which depict excellent analytical figure of merits (i.e, precision, selectivity, sensitivity, etc). Dilution of real samples actually helped mitigate matrix effect approximating their behavior identical to aqueous samples. As a matter of fact, slopes of calibration equations of all dilute real samples studied were found very close to that of aqueous sample (Tables 1 and 2). Interestingly, slopes (sensitivities) for Cu(II) are found always higher than those of Cd(II). This indicated the peak current for Cd(II) increased linearly like that of Cu(II) but at a slower rate. A satisfactory agreement between the declared analyte content and determined value for the pharmaceutical sample (Table 2) endorses quantitative recovery of the analyte and accuracy of the result by the proposed method (certified values for other real samples are not available).

3.9. Stability and reproducibility of the proposed sensor

The reproducibility and ruggedness of sol–gel–DIIP/PGE sensor were investigated to ensure the precision and practicability of the method. (For details, vide Supplementary material section S6). The proposed method was validated by the comparison of amounts of Cd(II) and Cu(II) recovered from aqueous samples with those of a standard HMDE procedure [25] exploiting DPASV sensing. Both the methods revealed quantitative (100%) recoveries of Cd(II) and Cu (II) in aqueous sample. Furthermore, the Student's t-test, where t_{cal} values (2.99 for Cd(II) and 2.22 for Cu(II)) were found to be less than t_{tab} (4.30) at the confidence level 95%, revealed that although a similar order of precision in the final result was realized by both methods, our method is relatively selective and sensitive to diagnose several associated chronic diseases (mentioned in the introduction part) manifested at the stringent limits of detection. Note that mercury-based electrodes have environmental issues

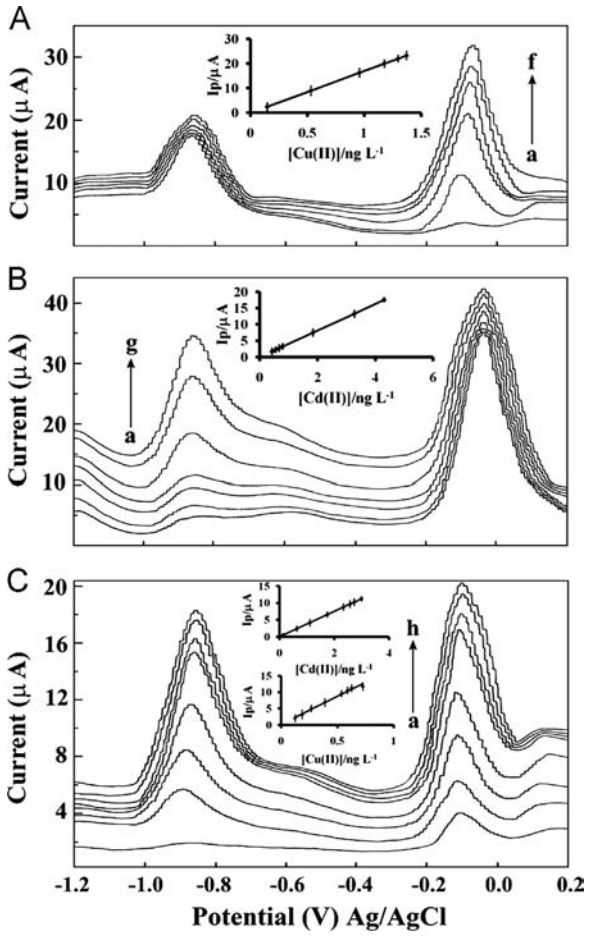

Fig. 4. (A) DPASV runs of Cu(II) at sol–gel–DIIP/PGE in the presence of 2.621 ng mL^{-1} (fixed) Cd(II) ion in acetate buffer (pH 5.5). Cu(II) concentrations (from a to f): 0.146, 0.529, 0.955, 1.174, 1.295 and 1.369 ng mL^{-1}. (B) DPASV runs of Cd(II) at sol–gel–DIIP/PGE in the presence of 1.815 ng mL^{-1} (fixed) Cu(II) ion in acetate buffer (pH 5.5). Cd(II) concentrations (from a to g): 0.429, 0.553, 0.675, 0.796, 1.846, 3.277 and 4.305 ng mL^{-1}. (C) DPASV runs obtained for the simultaneous analysis of Cd(II) and Cu(II) at sol–gel–DIIP/PGE in acetate buffer (pH 5.5). Cd(II) contents (from a to h): 0.124, 0.639, 1.118, 1.747, 2.333, 2.576, 2729, and 2.989 ng mL^{-1} Cu(II) contents (from a to h): 0.124, 0.187, 0.269, 0.388, 0.537, 0.59, 0.625, and 0.725 ng mL^{-1}. (Operating conditions: E_{acc} −1.2 V, t_{acc} 150 s, supporting electrolyte acetate buffer (0.1 M, pH 5.5), pulse amplitude 25 mV, scan rate 10 mV s^{-1}).

related to the use and disposal of toxic mercury. HMDE-based sensors cannot be practical, particularly for in-field investigations owing to their mechanical instability during various steps of assay procedure [69,70]. The proposed sensor was also compared with other reported methods for simultaneous determination of Cd(II) and Cu(II) (Table S2). Accordingly, the previously reported solid sensors had relatively poor sensitivity and some of them suffered from massive interferences. The present sensor is simple, cost-effective, and disposable and assures ultra-trace simultaneous assay of Cd(II) and Cu(II) in real samples, without any cross-reactivity and false-positives. As a matter of fact, there were absolutely no interferences observed from various interferents viz., dopamine (DA), ascorbic acid (AA), Fe(III), Mg(II), Hg(II), Mn(II), Pb(II), Zn(II), Co(II), Ni(II), either individually or concomitantly present in clinically relevant ratios with test analytes, in the present investigation. Furthermore, in spite of relatively sluggish binding kinetics of Cd(II) vis-a-vis Cu(II) binding, Fig. S6(B) fully endorses the analyte binding efficiency of DIIP to be non-competitive between both metal analytes or among metal analytes and interferent(s). (For details on cross-reactivity, vide Supplementary material section S7 and Fig. S6(A–B)).

4. Conclusion

The double ion-imprinting could be a suitable technique to combat inter-metallic complications during the course of simultaneous analysis of pairs of metal ions, in real-world samples. For the first time, a dual ion-imprinted polymer was prepared evolving its embedded sol–gel nano-film for the development of modified solid sensor. Dual imprinted cavities were found to weaken inter-metallic compound formation owing to their inherent imprinting impact exerting stronger analyte binding affinity. Under such conditions, the common problem of inter-metallic interactions between the two metal ions is largely obviated, insofar as simultaneous analysis is concerned. The proposed sol–gel – DIIP/PGE is reproducible, rugged, renewable, and cost-effective in which imprinted cavities of the film were found to be highly selective, responding an independent analyte binding and thereby the quantitative detection of Cd(II) and Cu(II) simultaneously, at ultra trace levels. This avoided any bias and equivocal data on account of inter-metallic interactions between Cd(II) and Cu(II) ions in real samples.

Acknowledgments

Authors thank the Council of Scientific and Industrial Research-University Grant Commission (CSIR-UGC), New Delhi for granting senior research fellowship to one of us (DJ). Instrumental facilities helps were procured out of a recent project (SR/S1/IC-30/2010) funded by the Department of Science and Technology, New Delhi. The financial help was rendered in the form of junior research fellowship to AV (CSIR project sanction no. 01/2319/09/EMR-II).

Appendix A. Supplementary material

Supplementary data associated with this article can be found in the online version at http://dx.doi.org/10.1016/j.talanta.2013.12.036.

References

[1] L. Wang, G. Xue, M. Zhou, L. Wang, Y. Chen, J. Yuan, IEEE (2009).
[2] T. Moreau, G. Orssaud, J. Lellouch, J.R. Claude, B. Juguet, B. Festy, Arch. Environ. Health 38 (1983) 163–167.
[3] E.E. Grum, E.A. Brestnitze, Cadmium Toxicity, U.S Department of Health and Human Services, California, 1991.
[4] K. Nogwa, T. Kido, Chiba Igaka Zasshi 66 (1991) 1–8.
[5] L. Guanghan, L. Dewu, L. Dehua, Z. Tong, Z. Hongyan, L. Chuanyin, Food Chem. 84 (2004) 319–322.
[6] M.B. Gholivand, A. Sohrabi, S. Abbasi, Electroanalysis 19 (2007) 1609–1615.
[7] ⟨http://www.bloodbook.com/ranges.html⟩, 07/11/2013.
[8] L.M. Klevay, Mayo Clin. Proc. 81 (2006) 132. (132).
[9] T.R. Halfdanarson, N. Kumar, C.Y. Li, R.L. Phyliky, W.J. Hogan, Eur. J. Haematol. 80 (2008) 523–531.
[10] H. Kodama, C. Fujisawa, Metallomics 1 (2009) 42–52.
[11] J.D. Hem, Study and Interpretation of the Chemical Characteristics of Natural Water, 2nd edn., US Department of the Interior, US Government Printing Office, Washington, 1960.
[12] I. Bremner, Am. J. Clin. Nutr. 67 (1998) 1069S–1073S.
[13] E. Shams, A. Babaei, M. Soltaninezhad, Anal. Chim. Acta. 501 (2004) 119–124.
[14] WHO (World Health Organization), Fifty-third report of the Joint FAO/WHO Expert Committee on Food Additives, WHO technical report series 896, Geneva, Switzerland, 2000.
[15] H.A. Wise, D.A. Roston, W.R. Heineman, Anal. Chim. Acta 154 (1983) 95–104.
[16] A.A. Ensafi, T. Khayamian, A. Benvidi, E. Mirmomtaz, Anal. Chim. Acta 561 (2006) 225–232.
[17] J.F. van Staden, M.C. Matoetoe, Anal. Chim. Acta 411 (2000) 201–207.
[18] I.B. Velasquez, G.S. Jacinto, F.S. Valera, Mar. Pollut. Bull. 45 (2002) 210–217.
[19] M.H. Matloob, A.M. Al-Joufi, A.A.S. Al-Badani, E.M.K. Eqlan, Qatar Univ. Sci. J. 24 (2004) 91–100.
[20] D. Sancho, L. Deban, R. Pardo, D. Valladolid, J. Sci. Food Agric. 85 (2005) 1021–1025.
[21] A.C.V. dos Santos, J.C. Masini, Anal. Bioanal. Chem. 385 (2006) 1538–1544.
[22] A. Babaei, M. Babazadeh, E. Shams, Electroanalysis 19 (2007) 978–985.
[23] A.M. Beltagi, M.M. Ghoneim, J. Appl. Electrochem. 39 (2009) 627–636.

[24] S. Arab, A. Alshikh, J. Am. Sci. 6 (2010) 1026–1032.
[25] S. Abbasi, A. Bahiraei, F. Abbasai, Food Chem. 129 (2011) 1274–1280.
[26] J. Jakumnee, S. Suteerapataranon, Y. Vaneesorn, K. Grudpan, Anal. Sci. 17 (2001) i399–i401.
[27] M.F. de Oliveira, A.A. Saczk, L.L. Okumura, A.P. Fernandes, M. de Moraes, N.R. Stradiotto, Anal. Bioanal. Chem. 380 (2004) 135–140.
[28] M.F.M. Noh, I. Tothill, Sains Malaysia Malays 40 (2011) 1153–1163.
[29] W. Yantasee, Y. Lin, G.E. Fryxell, B.J. Buscheet, Anal. Chim. Acta 502 (2004) 207–212.
[30] F. Xia, X. Zhang, C. Zhou, D. Sun, Y. Dong, Z. Liu, J. Autom. Methods Manage. (2010) 1–6.
[31] A.M. Beltagia, E.M. Ghoneimb, M.M. Ghoneim, Intern. J. Environ. Anal. Chem. 91 (2011) 17–32.
[32] C. Truzzi, A. Annibaldi, S. Illuminati, E. Bassotti, G. Scarponi, Anal. Bioanal. Chem. 392 (2008) 247–262.
[33] B.B. Prasad, D. Jauhari, M.P. Tiwari, Biosens. Bioelectron. 50 (2013) 19–27.
[34] C. Dai, J. Zhang, Y. Zhang, X. Zhou, Y. Duan, S. Liu, Environ. Sci. Pollut. Res. 20 (2013) 5492–5501.
[35] Y. Guo, T. Guo, Chem. Commun. 49 (2013) 1073–1075.
[36] J. Matsui, T. Sodeyama, K. Tamakib, N. Sugimoto, Chem. Commun. 20 (2006) 3217–3219.
[37] T. Jing, Y. Wang, Q. Dai, H. Xia, J. Niu, Q. Hao, S. Mei, Y. Zhou, Biosens. Bioelectron. 25 (2010) 2218–2224.
[38] K. Sreenivasan, J. Appl. Polym. Sci. 82 (2001) 889–893.
[39] R. Suedee, V. Seechamnanturakit, A. Suksuwan, B. Canyuk, Int. J. Mol. Sci. 9 (2008) 2333–2356.
[40] M.P. Tiwari, R. Madhuri, D. Kumar, D. Jauhari, B.B. Prasad, Adv. Mater. Lett. 2 (2011) 276–280.
[41] J. Xin, X. Qiao, Z. Xu, J. Zhou, Food Anal. Methods 6 (2013) 274–281.
[42] R. Kala, T.P. Rao, J. Sep. Sci. 29 (2006) 1281–1287.
[43] H. Nishide, J. Deguchi, E. Tsuchida, Chem. Lett. (1976) 169–174.
[44] C. Branger, W. Meouche, A. Margaillan, Recent advances on ion-imprinted polymers, React. Funct. Polym. 73 (2013) 859–875.
[45] D. Kumar, R. Madhuri, M.P. Tiwari, P. Sinha, B.B. Prasad, Adv. Mater. Lett. 2 (2011) 294–297.
[46] S.M. Macdonald, K. Szot, J. Neidziolka, F. Marken, M. Opallo, J. Solid State Electrochem. 12 (2008) 287–293.
[47] B.B. Prasad, D. Kumar, R. Madhuri, M.P. Tiwari, Biosens. Bioelectron. 28 (2011) 117–126.
[48] D.A. Skoog, F.T. Holler, T.A. Neiman, Principles of Instrumental Analysis, 5th ed., Harcourt Brace College Publishers, Orlando, 1998.
[49] K.K. Kannan, B. Notstrand, K. Fridborg, S. Lovgren, A. Ohlsson, M. Petef, Proc. Natl. Acad. Sci. USA 72 (1975) 51–55.
[50] A. Liljas, K.K. Kannan, P.C. Bergstén, I. Waara, K. Fridborg, B. Strandberg, V. Carlbom, L. Järup, S. Lövgren, M. Petef, New Biol. 235 (1972) 131–137.
[51] M.L. Ludwig, W.N. Lipscomb, in: G.L. Eichhorn (Ed.), Inorganic Biochemistry, vol. II, Elsevier, Amsterdam, 1973 (Chapter 22).
[52] B.W. Matthews, L.H. Weaver, Biochemistry 13 (1974) 1719–1725.
[53] J.S. Richardson, K.A. Thomas, B.H. Rubin, D.C. Richardson, Proc. Natl. Acad. Sci. USA 72 (1945) 1349–1353.
[54] S.J. Lau, B. Sarkar, J. Biol. Chem. 246 (1971) 5938–5943.
[55] P.M. May, P.W. Linder, D.R. Williams, J. Chem. Soc. Dalton Trans. (1977) 588–595.
[56] T. Szabo-Planka, A. Rockenbauer, L. Korecz, D. Nagy, Polyhedron 19 (2000) 1123–1131.
[57] X. Gao, Handbook on the Physics and Chemistry of Rare Earths, vol. 8, Elsevier Science Publishers B.V (1986) 163–201.
[58] R.N. Patel, N. Singh, R.P. Shrivastava, K.K. Shukla, P.K. Singh, Proc. Indian Acad. Sci. (Chem. Sci.) 114 (2002) 115–124.
[59] Q. Hu, E. Marand, Polymer 40 (1999) 4833–4843.
[60] L.Y. Beaulieu, A.D. Rutenberg, J.R. Dahn, Microsc. Microanal. 8 (2002) 422–428.
[61] B.B. Prasad, I. Pandey, Sens. Actuators B 186 (2013) 407–416.
[62] H. Ju, D. Leech, J. Electroanal. Chem. 484 (2000) 150–156.
[63] G.E. Batley, T.M. Florence, J. Electroanal. Chem. 55 (1974) 23–43.
[64] T.M. Florence, J. Electroanal. Chem. 35 (1972) 237–245.
[65] S.T. Crosum, J.A. Dean, J.R. Stokely, Anal. Chim. Acta 75 (1975) 421–430.
[66] P. Ostapczuk, Z. Kublik, J. Electroanal. Chem. 83 (1977) 1–17.
[67] M. Lin, M.S. Cho, W.S. Choe, Y. Lee, Biosens. Bioelectron. 25 (2009) 28–33.
[68] E. Laviron, J. Electroanal. Chem. 101 (1979) 19–28.
[69] J. Wang, J. Wang, B. Tian, M. Jiang, Anal. Chem. 69 (1997) 1657–1661.
[70] J. Wang, J. Lu, D.D. Larson, K. Olsen, Electroanalysis 7 (1995) 247–250.